07,05

Mechanosynthesised $(Fe,Cr,Si)_{75}C_{25}$ alloy: phase composition and redistribution of alloying elements as a result of thermal effects

© A.A. Chulkina, A.I. Ulyanov

Federal State Budgetary Scientific Organisation Udmurt Federal Research Center
of the Ural Branch of the Russian Academy of Sciences,
Izhevsk, Russia

E-mail: chulkina@udman.ru

Received July 24, 2024
Revised November 29, 2024
Accepted December 29, 2024

The structural and phase analysis of as-mechanosynthesized and subsequently annealed $(Fe_{1-x-y}Cr_xSi_y)_{75}C_{25}$ alloys, where $x = 0.05, 0.10$, $y = 0.01, 0.03$, was performed using X-ray diffraction, differential scanning calorimetry and magnetic measurements. During mechanosynthesis, a large amount of X-ray amorphous phase is formed, which crystallizes in two stages during annealing. One of the components of crystallization is cementite. After the first stage of crystallization (annealing temperature up to 500 °C), the concentration of chromium in cementite is practically independent of the silicon content, and is determined only by the chromium content in the alloys. As a result of the second crystallization stage of the residual X-ray amorphous phase and annealing at 800 °C, a quite homogeneous alloyed cementite is formed, the chromium concentration in which is determined by both Cr and Si content in the alloys.

Keywords: mechanosynthesis, nanostructured materials, phase transitions, phase composition, annealing, redistribution of alloying elements.

DOI: 10.61011/PSS.2025.03.60882.204

1. Introduction

Cementite, being a metastable phase, is commonly included into the composition of industrial steels, substantially impacting their mechanical properties [1]. However, in such steels cementite is practically always different by its chemical composition from the stoichiometric ratio of Fe_3C. It may be doped with carbide-promoting elements, for example, chromium. Doping of steels with chromium considerably improves the thermal stability of cementite [2]. Besides, chromium increases the impact resistance and corrosion resistance of steels. But at the same time steel doping with this element introduces certain negative moments to the properties of steels — decreases their plasticity and linear expansion ratio.

Steels are doped with non-carbide-promoting elements, too. It is assumed that they, being in a solid solution, form no carbides, but decrease their thermal stability, promoting steel graphitization. Such elements include silicon. Silicon, as chromium, improves strength, hardness and electrical resistance of steels. Silicon helps to improve heat resistance and limit of elasticity of steel. Silicon plays a special role in carbon, especially martensite, steels. It helps to delay the growth of cementite precipitations [3,4]. In [5] it is shown that in steel Fe−1.5Cr−1.0C with silicon content from 0.42 to 0.71 wt.% a layer of Si atoms is formed around the cementite particles, which prevents diffusion of carbon atoms and growth of cementite inclusions.

In [6–8] the results are presented from the numerical modeling of Si impact at the cementite formation energy. These papers studied the options of silicon substituting the positions of both iron and carbon atoms. It was obtained that for all positions of Si atoms in the cementite cell the partial enthalpy is positive. It would follow that silicon must stay in the solid solution BCC-Fe, and not in the cementite lattice. Nevertheless, the conclusions received from the theoretical calculations, require experimental testing. It turned out that it was possible to produce experimentally the silicon-doped cementite. In [9] the methods of transmission electron microscopy and atom probe tomography were used to study the nanocrystalline steel with composition $Fe_{89.57}Mn_{1.82}Cr_{1.28}Mo_{0.14}V_{0.09}C_{4.34}Si_{2.76}$ at.%. It was found that one-hour tempering at 400 °C led to formation of cementite particles from the solid solution without redistribution of doping elements. After such tempering the average concentration of silicon in cementite was 3.14 at.%, and in ferrite — 3.44 at.%. Half-hour-tempering at 450 °C decreases the content of Si in cementite to 2.11 at.%, and hour-tempering at 550 °C — practically down to zero. Therefore, the silicon in the process of annealing at 550 °C and above quickly diffuses from cementite.

Silicon-doped cementite was also produced by the method of severe plastic deformation, in particular, by mechanical synthesis (MS) in a ball planetary mill [10]. Based on the analysis of cementite stability with the increase of the Si content in the alloys based on $Fe_{75}C_{25}$ the conclusion was made that cementite produced under MS conditions was doped with silicon. Cementite stability to thermal exposure in silicon-containing alloys may be provided by introduction of chromium into its composition [2].

The purpose of this paper is to study the formation of phases and patterns of Cr and Si doping elements redistribution between phases in the process of heating and annealing of mechanically synthesized nanocrystalline alloys with composition $(Fe,Cr,Si)_{75}C_{25}$.

2. Specimens and research methods

Alloys with cementite composition $(Fe_{1-x-y}Cr_xSi_y)_{75}C_{25}$, where $x = 0.05$ and 0.10, $y = 0.01$ and 0.03, were prepared from powders of carbonyl Fe of grade OSCh 13-2 (purity 99.98 %), Cr (99.9 %), Si (99.999 %) and hexagonal graphite (99.99 %). The original mixture of powders was exposed to high energy impact in the protective atmosphere of argon in a ball planetary mill Pulverisette-7. The specific capacity of the mill at platform rotation speed of 74 rad/c equals 2 W/g. Due to forced air cooling the heating of milling pots, grinding balls and powder in process of mill operation did not exceed 60 °C. The mass of the original powder mix was 10 g. The ratio of the mass of grinding balls with diameter of 8 mm to the mass of the loaded powder was 7 : 1. Milling yield from the walls of the milling pots with volume of 45 cm^3 from steel ShH-15 and surface of the balls of the same material at MS time of 16.5 h did not exceed 3–4 wt.%.

Mechanically synthesized specimens were annealed in an argon atmosphere at an installation to measure temperature dependence of magnetic susceptibility $\chi(T)$. The amplitude of the probing alternating magnetic field was 1.25 A/cm, frequency — 120 Hz. Dependence $\chi(T)$ was measured in the process of heating to the specified temperature, one-hour soaking and cooling of the specimen to the room temperature. The value of magnetic susceptibility in the curves is given in relative units χ/χ_{20}, where χ — current, and χ_{20} — measured in the process of heating at 20 °C value of the specimen magnetic susceptibility.

X-ray diffraction patterns were produced using diffractometer Miniflex 600 (Rigaku) under CoK_α-radiation in Bragg–Brentano geometry with the rate of 2 deg/min. Measurement temperature — is room temperature. Quantitative X-ray diffraction analysis was carried out using a software suite [11]. The value of microdeformations of the lattices $\langle\varepsilon^2\rangle^{1/2}$ was determined using the modified method of Warren–Averbach [12], with formula

$$\langle\varepsilon^2\rangle^{1/2} = \frac{\beta_G^\Phi}{2\sqrt{2\pi}l_0 \operatorname{tg}\theta_0},$$

where θ_0 is peak maximum position, $l_0 = \sqrt{H^2+K^2+L^2}$, H, K, L is indices of crystallographic planes, β_G^Φ is integral width of Gaussian component of physical broadening of line profile (in radians). The physical width of lines was calculated using formula $\beta_G^\Phi = \sqrt{(\beta_G^e)^2-(\beta_G^i)^2}$, where β_G^e and β_G^i is accordingly the experimental and instrumental widths. The reference for definition of the instrumental broadening of the lines was a diffraction pattern α-SiO_2, obtained in the same modes of registration as the specimen diffraction patterns.

Dependence of the coercive force H_c on measurement temperature T was estimated using a vibration magnetometer with the maximum magnetizing field of 13 kA/cm. The measurement temperature was decreased, starting from the room one, down to — 196 °C.

Differential scanning calorimetry (DSC) was carried out on installation DSC 404 C Pegasus by Netzsch with the operating temperature range from 30 to 1500 °C. Experiments were carried out in corundum crucibles in the protective argon atmosphere (after prior pumping of the working chamber to 10^{-3} Pa).

Modes of thermal treatment of the studied mechanically synthesized specimens are provided in Table 1.

3. Results and discussion

Figure 1 presents for comparison the X-ray diffraction patterns of alloys Cr5Si3 and Cr10Si3 after MS, and also subsequent annealings at temperatures $T_{ann} = 500$, 600 and 800 °C. The phase composition of low-silicon alloys $(Fe_{0.99-x}Cr_xSi_{0.01})_{75}C_{25}$ and alloys with higher silicon content $(Fe_{0.97-x}Cr_xSi_{0.03})_{75}C_{25}$, where $x = 0.05$ and 0.10, depending on the annealing temperature, obtained as a result of X-ray data processing, is presented accordingly in Table 2 and in Figure 2. Let us compare the obtained results for the mechanically synthesized alloys (in Table and figure such state is indicated as annealing at room temperature $T_{ann} = 20$ °C). In contrast to low-silicon alloys, where around 36–39 vol.% cementite and 10–17 vol.% χ-carbide (Fe_5C_2) are formed, the alloys with the higher content of silicon demonstrate a reverse ratio of these phases: up to 39 vol.% of Hagg's carbide and only 9–11 vol.% cementite. The disordered X-ray amorphous phase (XAP) is abundant in all alloys, from 40 to 58 vol.%. Several percent falls upon α-Fe (or ferrite — solid solution of carbon and other elements in α-Fe). Let us discuss the reasons for such great difference in the ratio of phases of the discussed alloys produced in process of MS.

It is known that [13] at the initial stage of MS of the original powder mix with composition $Fe_{75}C_{25}$, consisting of iron with grade OSCh 13-2 with particle size to 300 μm and graphite with purity of 99.99 %, α-Fe changes to nanocrystalline state with non-equilibrium boundaries, where carbon atoms are located as segregations. After achievement of the minimum grain size in process of MS and segregation saturation with carbon, XAP is formed. Its composition is gradually enriched with carbon to achieve the concentration close to 25 at.%, after which cementite is made. Formation of other carbides at the same time was not observed. However, MS of doped alloys based on $Fe_{75}C_{25}$ may cause formation of other carbides from XAP. As it follows from [14], if cementite release from XAP is delayed under the effect of impurities or for other reasons, in process of MS the composition of this phase will be

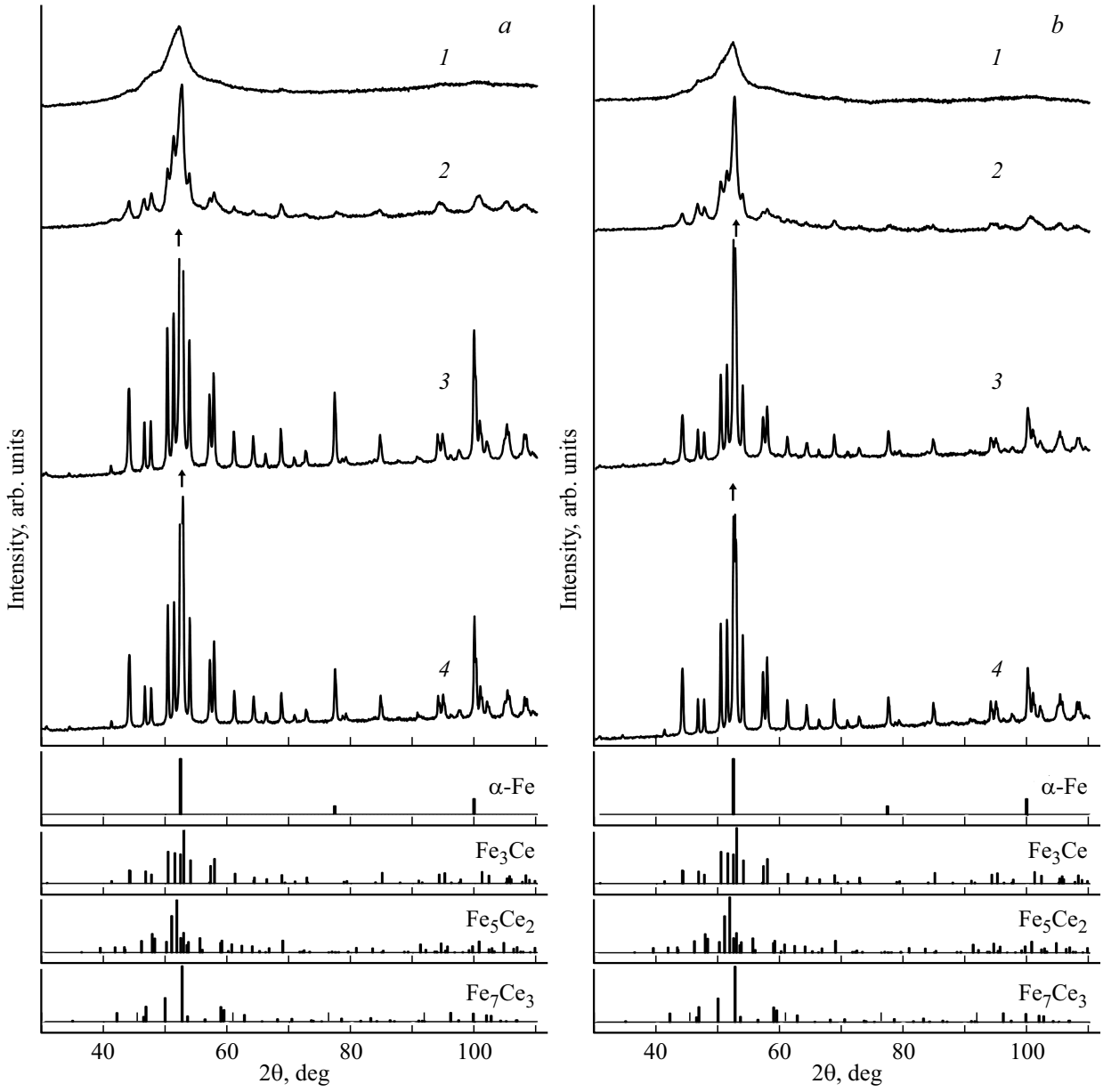

Figure 1. Diffraction patterns of alloys Cr5Si3 (*a*) Cr10Si3 (*b*) after MS (*1*) and annealing at temperatures T_{ann}: *2* — 500, *3* — 600, *4* —- 800°C.

Table 1. Atomic composition and conditions of thermal treatment of alloy specimens

Atomic composition of alloy	Designation alloy in the text of the article	Modes of thermal treatment of specimens				
		Annealing at installation for measurement of $\chi(T)$			DSC	
		Heating rate, deg/min	Temperature of annealing, T_{ann}, °C	Time of delay, h	Heating rate, deg/min	Range of change of temperature, °C
$(Fe_{0.94}Cr_{0.05}Si_{0.01})_{75}C_{25}$	Cr5Si1	30	200–800	1	10	40–700
$(Fe_{0.92}Cr_{0.05}Si_{0.03})_{75}C_{25}$	Cr5Si3					
$(Fe_{0.89}Cr_{0.10}Si_{0.01})_{75}C_{25}$	Cr10Si1					
$(Fe_{0.87}Cr_{0.10}Si_{0.03})_{75}C_{25}$	Cr10Si3					

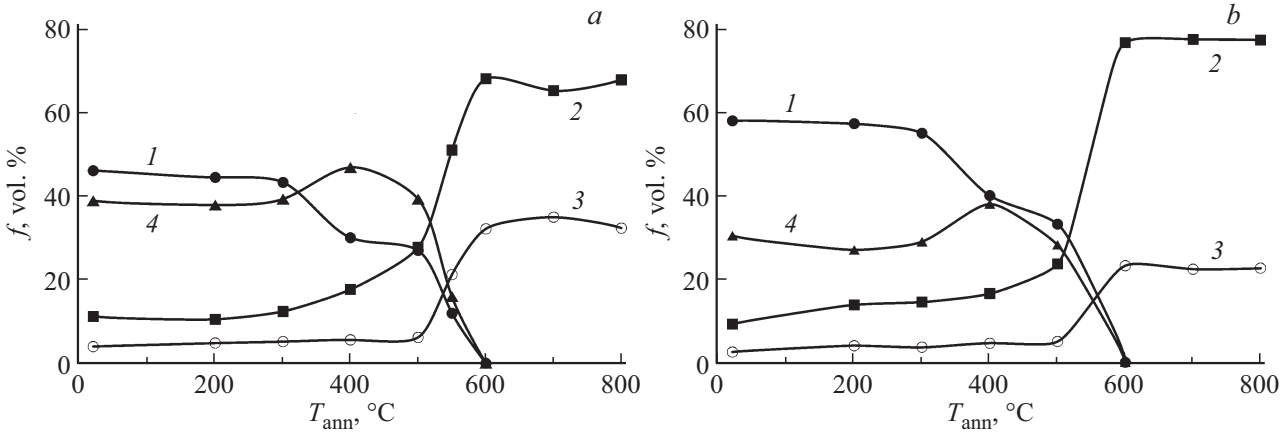

Figure 2. Dependence on annealing temperature T_{ann} in phase composition of alloys Cr5Si3 (*a*) and Cr10Si3 (*b*). Phases: *1* — X-ray amorphous phase (XAP), *2* — cementite, *3* — ferrite, *4* — Fe_5C_2 (after annealing at $T_{ann} = 400-500\,^{\circ}C$: $Fe_5C_2 + Fe_7C_3$).

Table 2. Phase composition of alloy specimens $(Fe_{0.99-x}Cr_xSi_{0.01})_{75}C_{25}$ after MS and annealing

T_{ann}, °C	Phases of alloys			
	α-Fe, vol.% ± 1	Fe_3C, vol.% ± 1	Fe_5C_2, vol.% ± 1	XAP, vol.% ± 1
$(Fe_{0.94}Cr_{0.05}Si_{0.01})_{75}C_{25}$				
20	5.1	38.5	16.6	39.8
500	6.3	93.7	–	–
800	6.7	93.3	–	–
$(Fe_{0.89}Cr_{0.10}Si_{0.01})_{75}C_{25}$				
20	3.2	36.1	10.4	50.3
500	4.1	95.9	–	–
800	7.2	92.8	–	–

enriched with carbon to the concentration above 25 at.%, and it becomes possible to form carbide Fe_5C_2. Therefore, after MS of doped alloys, one may observe phases of both cementite and χ-carbide. In our case the admixture that delayed substantially the release of cementite from XAP was silicon. The more silicon there is in the alloy, the more XAP is enriched with carbon. As a result, in the alloys with higher silicon content in process of MS XAP releases mostly χ-carbide (Figure 2). Accordingly, in low-silicon MS-alloys mostly cementite is formed (Table 2).

Thermal treatment causes changes in the phase composition of alloys. The differential scanning calorimetry (DSC) may be used to track the dynamics of phase conversion when mechanically synthesized specimens of the studied alloys are heated. Figure 3 presents the DSC curves (temperature dependences of the heat flux) of alloys Cr10Si1, Cr5Si3 and Cr10Si3. As it follows from the figure, after heating of the alloys to temperatures 240–300 °C, the exothermic process is launched, which supports XAP crystallization. Most unstable XAPs are contained in low-silicon alloys. Therefore, already at temperature 335 °C in the DSC curve of alloy Cr10Si1 (Figure 3, curve *1*) the first local maximum is formed, which indicates termination of intensive heat supply, which usually happens when carbides are formed from such phase. After temperature increases to 410 °C, heat release starts again. In this case, most probably, χ-carbide is converted to cementite [15], i. e. heat release supports the first-order conversion. Therefore, the peak with maximum at $T \approx 465\,^{\circ}C$ in the DSC curve describes conversion of χ-carbide. When heated above 500 °C, the released heat helps to form only a bend in the discussed curve in the area of temperature $\sim 550\,^{\circ}C$. Such nature of the DSC curve does not prevent further decomposition of the residual XAP into crystalline phases when temperature rises [16]. Residual XAP — a part of XAP left after release of carbides at annealings from $T_{ann} < 500\,^{\circ}C$. Low intensity of exothermic process may indicate small quantity of residual XAP in the discussed alloy.

In alloys with the higher silicon content the stage of carbide formation from XAP ends at higher temperatures

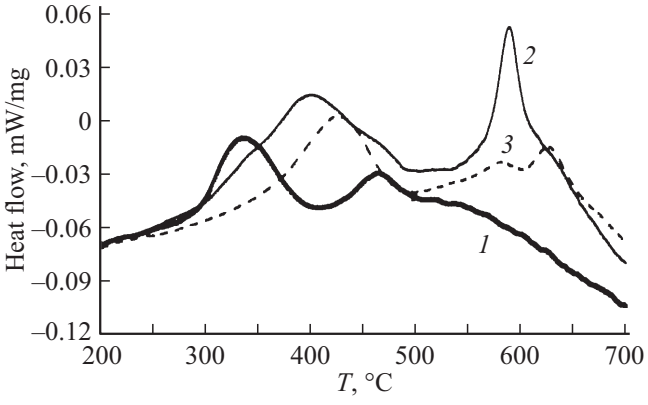

Figure 3. DSC thermograms in alloy heating: *1* — Cr10Si1, *2* — Cr5Si3, *3* — Cr10Si3.

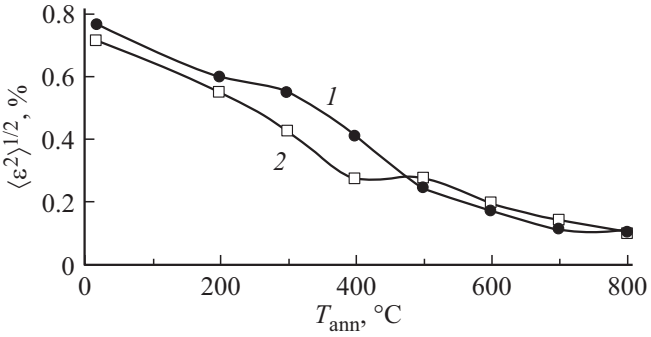

Figure 4. Dependence on annealing temperature T_{ann} in mean square microdeformation $\langle\varepsilon^2\rangle^{1/2}$ of crystalline lattices α-Fe (*1*) and cementite (*2*) of alloy Cr10Si3.

(Figure 3, curves *2* and *3*): the local maxima are fixed at $T = 400$ and 425 °C for compositions Cr5Si3 and Cr10Si3, accordingly. At the same time with this crystallization stage, in the alloys the χ-carbide changes to cementite, which manifests itself by a bend in curves *2* and *3* in the temperature area of $T = 465$ °C. At temperatures 500–550 °C heat release starts, which supports the crystallization of the residual XAP.

Increased time of soaking at this temperature in process of thermal treatment converts alloy phases into a more stable condition. Let us consider the impact of the temperatures of annealing conducted for 1 h, at the formation of phases of the studied mechanically synthesized alloys Cr5Si3 and Cr10Si3. It is possible to identify three temperature intervals differing in the nature of processes during annealing in dependences of phase composition on the annealing temperature T_{ann} of these alloys presented accordingly in Figure 2, *a* and *b*. In the first temperature range (annealing temperatures to 300 °C) the phase composition of alloys changes slightly, XAP (curves *1*) remains stable. Mainly the level of microdeformations of crystalline lattices of phases decreases, which is confirmed by Figure 4. In the figure for alloy Cr10Si3 there is dependence provided of mean square distortions $\langle\varepsilon^2\rangle^{1/2}$ of crystalline lattices α-Fe on the annealing temperature (curve *1*) and cementite (curve *2*). Similar trend of distortion decrease in the crystalline lattices of phases together with temperature rise is also observed in other studied alloys.

In the beginning of the second temperature interval ($T_{ann} \approx 300$–400 °C) only the carbon atoms, in contrast to the atoms of doping elements, may diffuse to large distances [17]. XAP is supersaturated with carbon compared to the stoichiometric composition of cementite, therefore, as a result of such thermal treatment it starts crystallizing and forms carbides Fe_3C and Fe_5C_2 (Figure 2, curves *2, 4*). Besides, in process of annealing at temperatures 400–500 °C XAP releases some carbide Fe_7C_3 (to ~ 2 and 10 vol.% in Cr5Si3 and Cr10Si3 alloys, accordingly). In Figure 2 the curve *4* reflects the total quantity of Hagg's and Fe_7C_3 carbides.

At temperatures $T_{ann} = 500$–600 °C (the end of the second temperature interval), when the diffusion mobility of atoms of alloy doping elements becomes rather high, the residual XAP gradually disintegrates to form most stable phases at these temperatures — ferrite and cementite. In the same range of annealing temperatures the carbides Fe_5C_2 and Fe_7C_3 are also converted to cementite [15,18]. The diffraction patterns of specimens annealed at $T_{ann} = 600$ °C also showed weak graphite lines. Therefore, after annealing at $T_{ann} = 600$ °C the alloys with higher silicon content are in a two-phase state (without the graphite traces). After annealing at temperatures up to 800 °C (third temperature interval, Figure 2) the alloys remain in two-phase state, and their volume content practically does not change.

In contrast to the alloys with the higher silicon content, the low-silicon alloys become two-phase (with account of error of phase composition detection at X-ray diffraction analysis) already after annealing at 500 °C (Table 1). After such thermal treatment the alloys consist of 94–96 vol.% cementite, and the rest — is ferrite. Increase of the annealing temperature to 800 °C weakly changes the ratio of these phases.

The studied alloys include Cr and Si as doping elements. In process of MS the atoms of these elements are distributed among formed phases. Let us discuss the redistributions of the doping elements when annealed in phases using the example of Cr10Si3 alloy, relying on the data of orthorhombic structure parameters change, i.e. change of the volumes of phase lattice cells. The change of the volume of cementite lattice cell V in this alloy depending on annealing temperature is shown in Figure 5 (curve *1*). Having analyzed the obtained dependence and taking into account the results of paper [19], let us confirm the location of atoms of doping elements both in mechanically synthesized and annealed cementite. It is known that the volume of the lattice cell of non-doped cementite Fe_3C decreases as the annealing temperature increases [16]. From the figure you can see that in the interval of the annealing temperatures 300–400 °C the volume of the cementite cell in the discussed alloy increases intensively. Chromium — carbide-promoting element. It will necessarily dope the mechanically synthesized cementite and cementite formed from XAP [2,20]. We assume that concentration of Cr in cementite up to $T_{ann} = 500$ °C does not vary substantially and has no impact at the nature of dependence $V(T_{ann})$. Taking into account the information on the silicon behavior in the cementite lattice in process of annealing (Si exits lattice) [9], one may assume that in this annealing temperature interval the silicon atoms are released from MS-cementite. This process is completed when annealed at $T_{ann} \approx 500$ °C. Let us prove this.

It is known that [21] the cementite lattice cell with parameters $a = 5.0896$, $b = 6.7443$, $c = 4.5248$ Å, including four formula units, contains twelve atoms of iron and four atoms of carbon. Iron atoms in the cementite lattice occupy two crystallographically nonequivalent positions: out of twelve

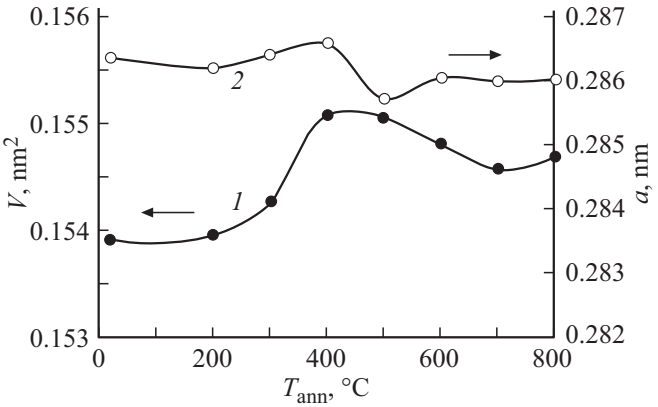

Figure 5. Dependences of volume V of cementite lattice cell (*1*) and parameter a of crystalline lattice α-Fe (*2*) on annealing temperature T_{ann} of Cr10Si3 alloy specimens.

Fe atoms, eight are located in the „main" position (8*d*), and four atoms — in „the special" position (4*c*). Carbon atoms may be located, according to [22], in four pores of the iron sublattice in the cementite crystalline lattice. Apart from „normal" prismatic and octahedral ones, these are „distorted" prismatic and octahedral pores.

In [19] they estimated the impact of options of substitution with doping elements of atoms of Fe and carbon occupying various positions in these carbides at the parameters of the cementite and Hagg's carbide unit cell. The volume of the cementite cell practically does not change, if the silicon atoms substitute iron, located in „the main" (8*d*) position of the cementite lattice cell, and decreases by $0.001-0.002\,\text{nm}^3$ in case of „special" (4*c*) position. The cell volume increases by $0.010-0.013\,\text{nm}^3$, if silicon substitutes carbon. Accordingly, if silicon occupying the position 4*c* of iron exits the cementite lattice, the lattice volume must increase, which is visualized by Figure 5 (curve *1*) in the interval $T_{ann} < 400\,^\circ\text{C}$. In case of silicon exit from the carbon position, the cementite cell volume must decrease. This contradicts the experiment results. Based on this, one may conclude that in process of MS-cementite formation the silicon atoms substitute the iron, and not carbon atoms. Numerical modeling [6] produced that the formation of the Si-doped cementite is energetically more beneficial when substituting Fe atoms from positions 8*d*, and not 4*c*. Nevertheless, this paper produced the results that do not prevent the possibility to form cementite, where silicon substitutes iron atoms not only from positions 8*d*, but also 4*c*.

The process of Si release in process of annealing happens not only from MS-cementite, but from χ-carbide. According to [19], the volume of χ-carbide cell when doped with silicon always increases, regardless of whether the iron or carbon positions are substituted. In particular, the volume of this carbide cell increases by $0.001-0.002$ and $0.01\,\text{nm}^3$ when silicon substitutes the Fe and carbon atoms, accordingly. It means that in case of Si atoms release from χ-carbide cell its volume must decrease. In this paper it was experimentally obtained that in process of χ-carbide rebuilding into cementite the volume of χ-carbide cell in Cr10Si3 alloy monotonically decreased by $\Delta V \approx 0.006\,\text{nm}^3$ with increase of T_{ann} to $500\,^\circ\text{C}$, which does not contradict the statement of silicon release from χ-carbide cell.

If T_{ann} increases, the interface zone from Si atoms formed around cementite [5] is damaged. The only phase, which may dissolve the considerable amount of silicon, is ferrite. Ferrite already in process of MS is doped with silicon, and also a certain amount of Cr (low compared to chromium concentration in cementite) [9]. It is known that [23] in the field of concentrations studied in this paper chromium increases the parameter of lattice α-Fe, and Si — decreases it. Change of a parameter of α-Fe lattice depending on T_{ann} of Cr10Si3 alloy is given in Figure 5 (curve *2*). From the figure you can see that at $T_{ann} > 500\,^\circ\text{C}$ the lattice parameter has lower values compared to the similar characteristic α-Fe of this alloy annealed at temperatures $T_{ann} < 400\,^\circ\text{C}$. Such change of parameter a of lattice α-Fe is related to increase of silicon concentration therein. After annealing at temperature above $500-600\,^\circ\text{C}$ all silicon of the alloy will be dissolved in ferrite as a result of damage of the interface zone from Si atoms formed around the cementite, and also crystallization of XAP. The substantial part of silicon from the composition is concentrated precisely in XAP of the alloy.

Note that as a result of annealing in interval $T_{ann} = 500-700\,^\circ\text{C}$ the volume of cell V of the chromium-doped cementite of Cr10Si3 alloy decreases (Figure 5, curve *1*). Similarly the non-doped cementite cell volume behaves with increase of T_{ann} [16]. However, decrease in dependence $V(T_{ann})$ of Cr10Si3 alloy cementite is caused by other factors too.

Let us consider the dependences of relative magnetic susceptibility on temperature of measurement $\chi(T)/\chi_{20}$ (polytherm) of the studied alloys. Polytherms $\chi(T)/\chi_{20}$ make it possible to both track the dynamics of phase formation and to assess the degree of doping the phases formed as a result of annealing at specified temperatures. Figure 6 presents curves $\chi(T)/\chi_{20}$ when heated to $800\,^\circ\text{C}$ (curves *1*), soaked at the specified temperature T_{ann} and subsequently cooled down to room temperature (curves *2–9*). The arrows indicate the temperature variation direction.

Let us start the discussion from the curves of soaking and cooling $\chi(T)/\chi_{20}$ of low-chromium alloy with higher silicon content Cr5Si3 (Figure 6, *c*, curves *2–9*). After annealing for 1 h at $T_{ann} = 400\,^\circ\text{C}$ we observe maxima and bends in the dependence (curve *2*), which are formed as a result of phase transition from paramagnetic to ferromagnetic state (Hopkinson effect [24]). After analysis of the position in the temperature axis of these maxima and bends, the phase Curie temperature may be predicted. We assume that the bend in temperature area $\sim 221\,^\circ\text{C}$ characterizes the XAP Curie temperature, maximum at $T \approx 172\,^\circ\text{C}$ — of Hagg's carbide, and another bend at $T \approx 123\,^\circ\text{C}$ — of cementite. When the annealing temperature increases, the quantitative ratio of phases changes. After annealing

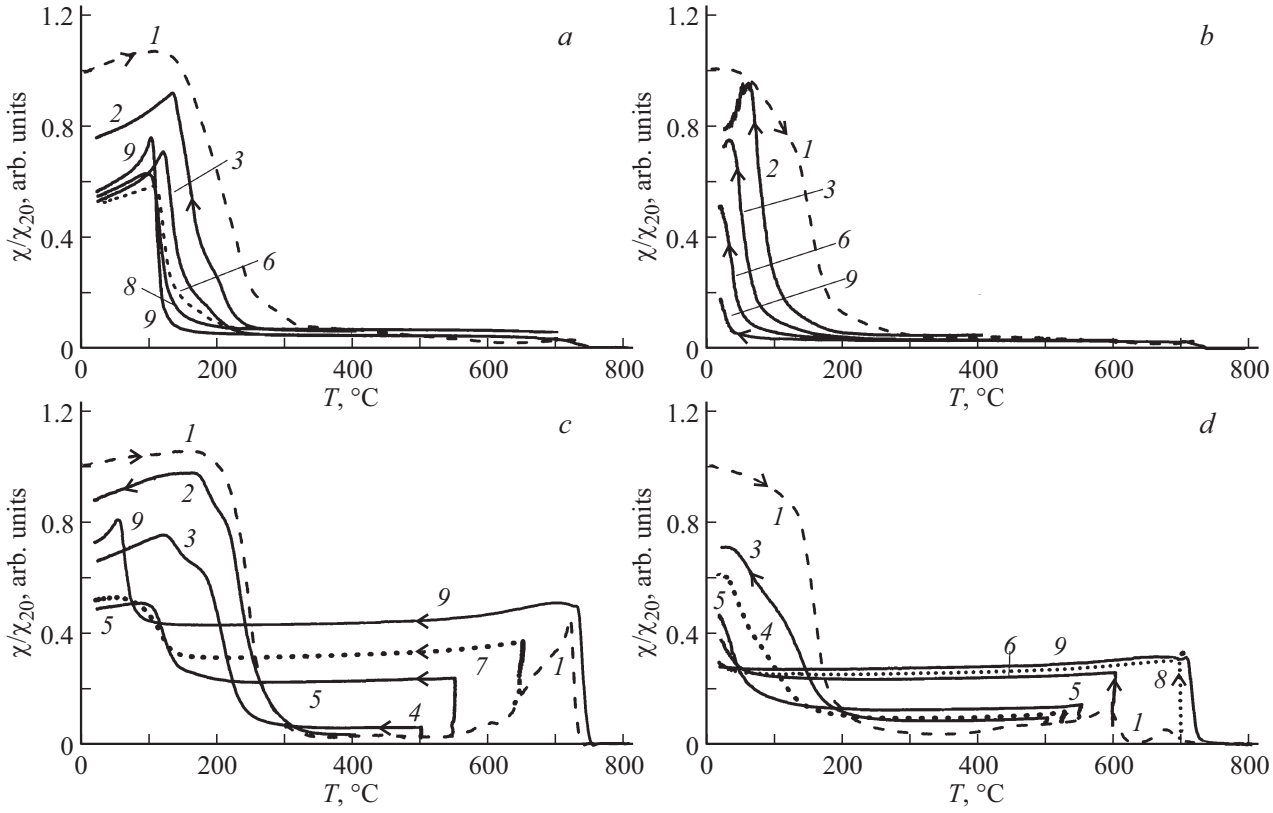

Figure 6. Relative magnetic susceptibility χ/χ_{20} of alloys $(Fe_{0.94}Cr_{0.05}Si_{0.01})_{75}C_{25}$ (*a*), $(Fe_{0.89}Cr_{0.10}Si_{0.01})_{75}C_{25}$ (*b*), $(Fe_{0.92}Cr_{0.05}Si_{0.03})_{75}C_{25}$ (*c*), $(Fe_{0.87}Cr_{0.10}Si_{0.03})_{75}C_{25}$ (*d*) depending on the heating temperature (curve *1*) and cooling after one-hour delay at temperatures T_{ann}: *2* — 400, *3* — 500, *4* — 525, *5* — 550, *6* — 600, *7* — 650, *8* — 700, *9* — 800 °C.

Table 3. Atomic composition and Curie temperature T_C of cementite in alloys annealed at temperatures T_{ann}, equal to 500 and 800 °C

Alloy	Curie temperature T_C of cementite in alloys, annealed at various temperatures, °C		Atomic composition of cementite in alloys, annealed at various temperatures, °C	
	$T_{ann} = 500$ °C	$T_{ann} = 800$ °C	$T_{ann} = 500$ °C	$T_{ann} = 800$ °C
Cr5rSi1	121	102	$(Fe_{0.95}Cr_{0.05})_3C$	$(Fe_{0.93}Cr_{0.07})_3C$
Cr5Si3	121	55	$(Fe_{0.95}Cr_{0.05})_3C$	$(Fe_{0.91}Cr_{0.09})_3C$
Cr10Si1	30	0	$(Fe_{0.90}Cr_{0.10})_3C$	$(Fe_{0.88}Cr_{0.12})_3C$
Cr10Si3	30	−75	$(Fe_{0.90}Cr_{0.10})_3C$	$(Fe_{0.85}Cr_{0.15})_3C$

at $T_{ann} = 500$ °C the curve *3* clearly shows the Hopkinson peak, which we use to determine the Curie temperature of the doped cementite — $T_C \approx 121$ °C. Note that cementite of low-chromium alloy with low content of silicon Cr5Si1 after similar annealing has T_C close to 121 °C (maximum in curve *3*, Figure 6, *a*).

Increasing the concentration of chromium in cementite reduces its Curie temperature [2]. In alloys with the increased content of chromium Cr10Si1 and Cr10Si3 after the annealing at 500 °C cementites have practically same Curie temperatures $T_C \approx 30$ °C (Figure 6, *b, d*, curves *3*).

As annealing temperature increases, cooling polytherms $\chi(T)/\chi_{20}$ (Figure 6) demonstrate smoothening and disappearance of bends responsible for XAP and χ-carbide. At the same time the maxima in curves *4*–*9*, which characterize the Curie temperature of cementite, are shifted towards lower temperatures. Besides, Hopkinson peaks of cementite gradually become more blurred (compare peaks in curves *3* and *6* (Figure 6, *a*), *5* and *7* (Figure 6, *c*)). Blurring of peaks in curves $\chi(T)/\chi_{20}$ is caused by increased heterogeneity of the doped cementite. One may assume that in the interval of the annealing temperatures 500–600 °C a fraction of cementite with higher concentration of chromium and accordingly lower Curie temperature appears in the alloys. Annealing at $T_{ann} = 800$ °C causes more homogeneous distribution of

chrome in cementite. Pronounced maxima are observed in the place of blurred peaks. Therefore, the transition of cementite from paramagnetic state to ferromagnetic one in the process of cooling of 800 °C annealed Cr5Si1 alloy happens at temperature $T_C \approx 102$ °C (Figure 6, *a*, curve *9*), and for the alloy with the same chromium content, but more silicon, Cr5Si3 — at $T_C \approx 55$ °C (Figure 6, *c*, curve *9*).

Curie temperatures T_C of alloys annealed at $T_{ann} > 500$ °C with higher chromium content $(Fe_{0.90-x}Cr_{0.10}Si_x)_{75}C_{25}$, where $x = 0.01$ and 0.03, are in the area of negative temperatures. To assess the T_C values, temperature dependences of coercive force $H_c(T)$, measured in the temperature interval from room temperature and to −196 °C, were used [25]. In Figure 7 such dependences are given for Cr10Si3 alloy. Arrows indicate the values T_C of cementite. From the figure it follows that after annealing of alloy at 800 °C cementite has $T_C \approx -75$ °C (curve *4*). Similar measurements were carried out for Cr10Si1 alloy. It was found that in cementite of alloy with low silicon content annealed at $T_{ann} = 800$ °C, $T_C \approx 0$ °C.

Let us assess the degree of cementite doping with chromium at its Curie temperature [2], assuming that after annealing at 500 °C it contains no silicon (Figure 5). The assessment results are reflected in Table 3, where Curie temperatures are given T_C and their corresponding atomic compositions of cementite in alloys annealed at temperatures of 500 and 800 °C.

To sum up the obtained results, one may conclude that in process of annealing at $T_{ann} \leq 500$ °C each of the studied alloys forms the chromium-doped cementite, the atomic composition of which is influenced by the content of chromium in the alloy, and is practically unaffected by silicon content therein. The situation varies when the annealing temperature increases. In the interval $500 < T_{ann} \leq 600$ °C in addition to the already available, cementite is formed with high chromium concentration. As a result, after annealing at $T_{ann} = 800$ °C the alloys contain a rather homogeneous cementite having a sharp Hopkinson peak in transition from the paramagnetic to the ferromagnetic state, and the concentration of chromium in cementite depends both on Cr content and Si content in the alloy. Curie temperature of cementite in the alloy annealed at 500 °C is higher than of T_C cementite of the same alloy, but annealed at $T_{ann} = 800$ °C.

Having obtained the new information on the additional doping of cementite with chromium in process of annealing at temperatures $T_{ann} > 500$ °C, let us again consider Figure 5 (curve *1*), which shows the dependence of the cementite lattice cell volume V in the alloy Cr10Si3 on the annealing temperature. As it follows from [19], substitution of Fe atoms with chromium must slightly decrease the volume of the cementite cell ($\Delta V < -0.001$ nm^3). The behavior of the experimental dependence $V(T_{ann})$ in the field $T_{ann} > 500$ °C (Figure 5, curve *1*) does not contradict the theoretical calculations [19]. Besides, in process of one-hour annealing of Cr10Si3 alloy at 800 °C, some Cr is released from cementite and then dissolved in ferrite, which causes increase of cementite Curie temperature (Figure 7, curves *3* and *4*, pay attention to arrows indicating the position T_C of cementite). Cementite cell volume V in this alloy after annealing at $T_{ann} = 800$ °C also increases (Figure 5, curve *1*).

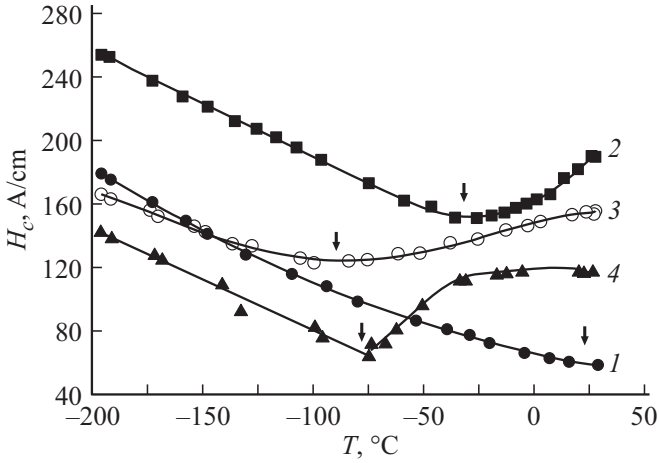

Figure 7. Dependence of coercive force on measurement temperature $H_c(T)$ of alloy specimens $(Fe_{0.87}Cr_{0.10}Si_{0.03})_{75}C_{25}$, annealed at T_{ann}: *1* — 500, *2* — 600, *3* — 700, *4* — 800 °C.

Having analyzed the obtained experimental data, one may state that in chromium alloys doped with silicon and obtained by MS method, XAP X-ray amorphous phase is crystallized in two stages when annealed. In the annealing temperature interval 300−500 °C the first stage of XAP crystallization is completed to form mostly carbide phases. In multi-component mechanically synthesized alloys after annealing approximately to 400−500 °C in virtue of limited diffusion mobility the heterogeneous distribution of doping elements is often maintained. Since silicon prevents origination of carbides [3,4], they grow in XAP areas depleted by silicon. Therefore, the carbide phases formed during the first stage of crystallization in process of annealing, are doped with Cr, but depleted by Si, in contrast to carbide phases released from XAP at high-energy treatment in process of MS and doped with both chromium and silicon. After the first stage of crystallization ($T_{ann} = 500$ °C) the residual XAP is enriched with silicon. Chromium concentration in the residual XAP will, most probably, be close to its concentration in XAP after MS.

In process of annealing at temperatures in the interval of $T_{ann} = 500-600$ °C the second stage of XAP crystallization takes place. The residual XAP is crystallized to form cementite and ferrite. All silicon and some chromium from residual XAP are dissolved in ferrite. And the main part of the Cr atoms contained in the residual XAP substitutes the iron atoms in the formed cementite, and its concentration is higher than in the cementite that is mechanically synthesized and formed at the first stage of XAP crystallization.

4. Conclusions

1. It was established that in process of mechanical synthesis of alloys $(Fe_{1-x-y}Cr_xSi_y)_{75}C_{25}$, where $x = 0.05$, 0.10, and $y = 0.01$, 0.03, composites were formed with the content of X-ray amorphous phase up to 40–58 vol.%. Besides, alloys with low content of silicon form 36–39 vol.% cementite and 10–17 vol.% χ-carbide. In alloys with higher silicon content — it is the opposite: χ-carbide is formed in the amount of up to 39 vol.%, and cementite — only 9–10 vol.%.

2. It was found that the X-ray amorphous phase of the studied alloys is crystallized in two stages. The first stage of crystallization at annealing temperatures $T_{ann} < 500\,^{\circ}C$ is characterized by formation of carbides from the sections of this phase with the minimum silicon content. During the second stage of crystallization ($T_{ann} = 500–600\,^{\circ}C$) of the residual X-ray amorphous phase, cementite is formed with higher concentration of chromium that in the previously formed cementite, and ferrite.

3. It is shown that after the completion of the first stage of crystallization of the X-ray amorphous phase, the chromium concentration in cementite practically does not depend on the Si content in the alloy and is determined only by content of chromium in it.

4. It was established that as a result of annealing at temperature $T_{ann} = 800\,^{\circ}C$ the cementite in the studied alloys became rather homogeneous, besides, chromium concentration in it depended both on Cr and Si content in the alloy.

5. It is shown that the process of silicon release from the mechanically synthesized cementite continues up to annealing temperatures $T_{ann} \approx 500\,^{\circ}C$. Redistribution of Si atoms previously contained in cementite and X-ray amorphous phase to ferrite occurs at higher annealing temperatures.

Acknowledgments

The authors wish to thank V.A. Volkov for X-ray diffraction analysis, L.V. Kamaeva for DSC-measurements and A.V. Zagainov for annealing of specimens.

Funding

The study was carried out using the equipment of the Shared Use Center „Center of Physical and Physicochemical Methods of Analysis and Study of Properties and Characteristics of the Surface, Nanostructures, Materials and Products“ of the Udmurt Federal Research Center of the Ural Branch of RAS within the framework of the state assignment of the Ministry of Science and Higher Education of the Russian Federation (No. of state registration 124021900079-9).

Conflict of interest

The authors declare that they have no conflict of interest.

References

[1] Tsementit v uglerodistykh stalyakh: kollektivnaya monografia / Pod red. V.M. Schastlivtseva. Izdatelstvo UMTs UPI, Yekaterinburg (2017). 380 s. (in Russian).
[2] A.A. Chulkina, A.I. Ulyanov, A.L. Ulyanov, I.A. Baranova, A.V. Zagainov, E.P. Yelsukov. Phys. Met. Metallogr. **116**, *1*, 19 (2015). DOI: https://doi.org/10.1134/S0031918X14100056.
[3] G. Miyamoto, J. Oh, K. Hono, T. Furuhara, T. Maki. Acta Mater. **55**, *15*, 5027 (2007). DOI: https://doi.org/10.1016/j.actamat.2007.05.023.
[4] B. Kim, C. Celada, D. San Martín, T. Sourmail, P.E.J. Rivera-Diaz-Castillo. Acta Mater. **61**, *18*, 6983 (2013). DOI: https://doi.org/10.1016/j.actamat.2013.08.012.
[5] T. Xu, Z. He, N. lv, X. Han, B. Wang, X. Hou. J. Mater. Sci. **57**, 22067 (2022). DOI: https://doi.org/10.1007/s10853-022-07996-x.
[6] J.H. Jang, I.G. Kim, H.K.D.H. Bhadeshia. Comput. Mater. Sci. **44**, *4*, 1319 (2009). DOI: https://doi.org/10.1016/j.commatsci.2008.08.022.
[7] A.V. Verkhovykh, A.A. Mirzoev, D.A. Mirzaev. Vestnik YuUrGU. Seriya „Matematika. Mekhanika. Physics“ **10**, *4*, 78 (2018). (in Russian). DOI: 10.14529/mmph180409.
[8] H. Sawada, K. Kawakami, F. Körmann, B. Grabowski, T. Hickel, J. Neugebauer. Acta Mater. **102**, 241 (2016). DOI: https://doi.org/10.1016/j.actamat.2015.09.010.
[9] F.G. Caballero, M.K. Miller, C. Garcia-Mateo, C. Capdevila, S.S. Babu. Acta Mater. **56**, *2*, 188 (2008). DOI: https://doi.org/10.1016/j.actamat.2007.09.018.
[10] V.A. Volkov, A.A. Chulkina, A.I. Ul'yanov, E.P. Elsukov. Phys. Met. Metallogr. **113**, *4*, 356 (2012). DOI: https://doi.org/10.1134/S0031918X12010140.
[11] E.V. Shelekhov, T.A. Sviridova. MiTOM **8**, 16 (2000). (in Russian).
[12] G.A. Dorofeev, A.N. Streletskii, I.V. Povstugar, A.V. Protasov, E.P. Elsukov. Colloid J. **74**, *6*, 678 (2012). DOI: 10.1134/S1061933X12060051.
[13] E.P. Elsukov, G.A. Dorofeev, V.M. Fomin, G.N. Konygin, A.V. Zagainov, A.N. Maratkanova. Phys. Met. Metallogr. **94**, 356 (2002).
[14] V.A. Volkov, A.A. Chulkina, I.A. El'kin, E.P. Elsukov. Phys. Met. Metallogr. **117**, *2*, 178 (2016). DOI: https://doi.org/10.1134/S0031918X15100142.
[15] V.A. Barinov, A.V. Protasov, V.T. Surikov. Phys. Met. Metallogr. **116**, *8*, 791 (2015). DOI: https://doi.org/10.1134/S0031918X15080025.
[16] E.P. Elsukov, V.M. Fomin, D.A. Vytovtov, G.A. Dorofeev, A.V. Zagainov, N.B. Arsent'eva, S.F. Lomaeva. Phys. Met. Metallogr. **100**, *3*, 251 (2005).
[17] G.V. Kurdyumov, L.M. Utevsky, R.I. Entin. Prevrascheniya v zheleze i stali. Nauka, M. (1977). 236 s. (in Russian).
[18] V.A. Barinov, V.A. Tsurin, V.T. Surikov. Phys. Met. Metallogr. **110**, *5*, 474 (2010).
[19] C.K. Ande, M.H.F. Sluiter. Metall Mater. Trans. A **43**, 4436 (2012). DOI: https://doi.org/10.1007/s11661-012-1229-y.
[20] A.A. Chulkina, A.I. Ulyanov, A.V. Zagainov, A.L. Ulyanov, E.P. Elsukov. Phys. Met. Metallogr. **116**, *3*, 293 (2015). DOI: 10.1134/S0031918X15030035.

[21] E.J. Fasiska, G.A. Jeffrey. Acta Crystallogr. **19**, *3*, 463 (1965). DOI: https://doi.org/10.1107/S0365110X65003602.
[22] A.V. Verkhovykh, K.Yu. Okishev, D.A. Mirzaev, A.A. Mirzoev. Vestnik YuUrGU. Seriya „Metallurgiya“ **18**, *4*, 34 (2018). (in Russian). DOI: 10.14529/met180404.
[23] A.V. Ponomareva. ZhETF **165**, *3*, 410 (2024). (in Russian). DOI: https://doi.org/10.31857/S0044451024030118.
[24] S. Tikadzumi. Fizika ferromagnetizma. Magnitnye kharakteristiki i prakticheskie primeneniya. Mir, M. (1987). 419 s. (in Russian).
[25] A.I. Ul'yanov, A.A. Chulkina, V.A. Volkov, E.P. Elsukov, A.V. Zagainov, A.V. Protasov, I.A. Zykina. Phys. Met. Metallogr. **113**, *12*, 1134 (2012). DOI: https://doi.org/10.1134/S0031918X12120137.

Translated by M.Verenikina